Original Article

The role of multimodal ultrasonic flow imaging in Thyroid Imaging Reporting and Data System (TI-RADS) 4 nodules

Libo Zhang[#], Junyi Gu[#], Yuxin Zhao, Min Zhu, Jing Wei, Bo Zhang

Department of Ultrasound, Dongfang Hospital, Shanghai, China

Contributions: (I) Conception and design: L Zhang; (II) Administrative support: B Zhang; (III) Provision of study materials or patients: J Gu; (IV) Collection and assembly of data: L Zhang; (V) Data analysis and interpretation: Y Zhao; (VI) Manuscript writing: All authors; (VII) Final approval of manuscript: All authors.

[#]These authors contributed equally to this work.

Correspondence to: Bo Zhang, MM. Department of Ultrasound, Dongfang Hospital, 150 Jimo Road, Shanghai 200120, China. Email: zpzhanglibo@hotmail.com; zpzhanglibo@outlook.com.

Background: Color Doppler imaging (CDFI), contrast-enhanced ultrasound (CEUS), and superb micro-vascular imaging (SMI) are used to observe blood flow characteristics in Thyroid Imaging Reporting and Data System (TI-RADS) 4 nodules. The ability of these techniques to distinguish benign from malignant nodules was investigated.

Methods: A total of 75 TI-RADS 4 nodules were examined using CDFI, SMI, and CEUS. The blood flow characteristics shown by the three methods were added to the current TI-RADS classification to establish a new TI-RADS classification. The value of the three methods and the diagnostic accuracy of the new and old TI-RADS classification were compared.

Results: SMI better captured type II flow in benign nodules and type III flow in malignant nodules relative to CDFI. Malignant nodules detected with CEUS manifested mainly with hypo-enhancement, whereas benign nodules showed iso- and hyper-enhancement. The areas under the receiver operating characteristic (ROC) curves (AUC) obtained through the aforementioned flow distribution models were 0.690 (CDFI), 0.840 (SMI), 0.910 (CEUS), and 0.903 (CEUS and SMI combined mode), respectively. The diagnostic value of CEUS was the highest. Joint inspection using SMI with CEUS showed certain advantages in sensitivity, although the overall accuracy was equal to that of CEUS alone. Except for CDFI, the AUC of the new TI-RADS classification was significantly higher than that of the old one. Perforating vessels and low enhancement were independent predictors of thyroid carcinoma.

Conclusions: Both SMI and CEUS visualized lower-velocity blood flow within TI-RADS 4 nodules. The new TI-RADS classification described here could improve diagnostic accuracy.

Keywords: Ultrasound; thyroid nodule; Thyroid Imaging Reporting and Data System (TI-RADS); superb micro-vascular imaging (SMI); contrast-enhanced ultrasound (CEUS)

Submitted Jul 09, 2020. Accepted for publication Aug 21, 2020.
doi: 10.21037/gs-20-641
View this article at: http://dx.doi.org/10.21037/gs-20-641

Introduction

Thyroid nodules are extremely common. Preoperative assessment of the nature of these nodules provides an important basis for the choice of therapeutic approaches. Ultrasound is used as the modality of choice for nodule detection. Radiologists evaluate the nature of thyroid nodules using the Thyroid Imaging Reporting and Data System (TI-RADS) classification based on the two-dimensional (2D) manifestation of the nodules. The TI-RADS classification proposed by Horvath in 2009 (1), which all thyroid nodules are divided into 6 categories.

It is based on the American Society of Radiology Breast Imaging Report and Data System (BI-RADS) (2). However, morphological images alone can be insufficient in accurately diagnosing nodule characteristics. Vessel distribution and flow characteristics within the nodules are widely believed to have a role in defining tumor characteristics (3-5). If tiny blood vessels are detected in a nodule, it indicates that the nodule has a malignant tendency. Therefore, the blood flow signs need to be included in the TI-RADS system evaluation. Microvascular imaging technology has also been applied to the TI-RADS system, and the combination of the two is used to identify malignant nodules. Current methods for depicting blood flow in thyroid nodules include color Doppler imaging (CDFI), contrast-enhanced ultrasound (CEUS), and superb micro-vascular imaging (SMI). CDFI is prone to lose low-frequency and low-velocity flow signal, whereas CEUS can image low flow signals with a diameter of 10–30 μm and a flow velocity of about 1 mm/s. However, the additional contrast agent needed for CEUS is expensive and poses a risk for allergic reaction. SMI was recently introduced as a noninvasive and economical technology for visualizing microflow and can favorably segment tissue signals and minimize motion artefacts. Despite these advantages, there are few reports regarding SMI efficacy in thyroid nodule characterization (6). Here, we observed the characteristics of nodule microvessels using CDFI, CEUS, and SMI, and compared differences between nodule inspection outcomes using single and multiple approaches to illustrate the potential value of SMI in TI-RADS 4 nodules.

We present the following article in accordance with the STARD reporting checklist (available at http://dx.doi.org/10.21037/gs-20-641).

Methods

Patients

A total of 57 consecutive patients (19 male and 38 female patients; mean age, 45.26±12.30; age range, 24–73 years) comprising 75 thyroid nodules were recruited between April 2016 and January 2018. The inclusion criteria were as follows: (I) confirmation of nodule pathology following surgical resection, and (II) classification of TI-RADS 4 by conventional ultrasound. Among the 75 nodules examined for this study, 55, 18, and 2 nodules were diagnosed as 4a, 4b, and 4c subclass, respectively. Nodules showing circular, coarse, and/or eggshell calcification that could influence SMI imaging were excluded from the study. Written informed consent was obtained from all study subjects. The study was conducted in accordance with the Declaration of Helsinki (as revised in 2013), and was approved by Shanghai East Hospital, Tongji University School of Medicine (No. 102).

Instruments and methods

Patients underwent ultrasonic examinations in the supine position with the neck sufficiently exposed. Each patient also was also clinically examined by CDFI, CEUS, and SMI to reveal additional information about localized microflow in the selected nodules. Two-D features of the thyroid nodules were observed, including size, morphology, border, internal echo, aspect ratio, and calcification. The collected 2-D features were then appraised according to guidelines recommended by the American College of Radiology, TI-RADS classification was executed, and nodules having a TI-RADS score of 4 were chosen. Sections with the most abundant flow according to CDFI were selected, and SMI technology was initiated. SMI was applied with a frame frequency of 25–45 fps, a depth of 4–5 cm, an image gain between 50% and 70%, a 2-D dynamic range of 50–65 dB, and a frequency of 7 Hz. CEUS was performed by injecting 1.5 mL of the ultrasound contrast SonoVue into the cubital vein. All examinations were performed by two experienced radiologists using an AplioTM 500 instrument equipped with a 5–14 MHz linear array probe. The first arm of the study involved defining the characteristics of the 2-D presentation in 75 thyroid nodules. In the second arm of the study, CDFI, SMI, and CEUS evaluation of the nodules was conducted. Finally, the results were recorded according to Digital and Imaging Communications in Medicine (DICOM) standards, and final decisions were reached by consensus.

Diagnostic criteria

TI-RADS was used to guide the diagnosis of thyroid nodules in this study (7). Kwak *et al.* (8) suggested that TI-RADS 4 nodules with solid echogenicity have the following ultrasound signs: hypoechoic/very hypoechoic, blurred border/spicular/irregular shape, microcalcification and aspect ratio >1, and can be divided into three subclasses: 4a, 4b, and 4c, which have one, two, and three or four signs, respectively. The vascular pattern in thyroid nodules can be divided into defined categories

Table 1 Assessment of the abundance of all nodules classified according to Kim *et al.*

Group	TI-RADS classification				χ^2	P
	I	II	III	IV		
CDFI	46	10	10	9	42.751	0.000
SMI	8	19	31	17		
χ^2	41.782	3.463	14.802	2.978		
P	0.000	0.063	0.000	0.084		

TI-RADS, Thyroid Imaging Reporting and Data System; CDFI, color Doppler flow imaging; SMI, superb microvascular imaging.

Table 2 Assessment of the abundance of benign nodules classified according to Kim *et al.*

Group	TI-RADS classification				χ^2	P
	I	II	III	IV		
CDFI	19	6	3	7	17.136	0.001
SMI	3	14	5	13		
χ^2	16.970	4.480	0.565	2.520		
P	0.000	0.034	0.452	0.112		

TI-RADS, Thyroid Imaging Reporting and Data System; CDFI, color Doppler imaging; SMI, superb micro-vascular imaging.

according to Kim *et al.* (5): type I, few (l–2 punctate or short rod signal) or absence of blood flow; type II, ≥3 peripheral vascularity; type III, ≥3 central vascularity; type IV, both type II and III characteristics. The contrast mode of the nodules can be characterized as having no enhancement, hypo-enhancement, iso-enhancement, or hyper-enhancement.

Here, we established a new TI-RADS classification, based on findings by several experienced radiologists and those reported in recent studies (9-12), which adds CDFI, SMI, and CEUS features to the old TI-RADS classification proposed by Kwak *et al.* In this updated TI-RADS classification, benign tendencies were deemed to present as iso-enhancement, hyper-enhancement or rim enhancement in CEUS and type II/IV flow in SMI, and thus downgraded the classification. In contrast, malignant tendencies would manifest as hypo-enhancement and type III flow, and in turn upgrade the classification. The remaining classifications remain unchanged. Using the updated TI-RADS, when the TI-RADS subclass results obtained by SMI and CEUS were not unanimous, the higher subclass was defined as the final result. Results obtained with the new classification were compared with those using the old TI-RADS classification.

Statistical analysis

Data analyses were conducted using SPSS 19.0 software, with a P value <0.05 considered to indicate statistical significance. Enumeration data between the two groups was checked by Chi-square test. To compare pathological results of the new and old TI-RADS classifications, sensitivity, specificity, and other indicators of CEUS, SMI, and CEUS + SMI were calculated, the receiver operating characteristic (ROC) curves were plotted, and the area under the curve (AUC) was compared by a Z test. Risk-scoring models for different ultrasound methods were built to filter real factors.

Results

Pathology

Among 75 thyroid nodules considered, pathological examination yielded 40 malignant nodules [papillary thyroid carcinoma (PTC), 2 with coexistent Hashimoto's thyroiditis and a maximum diameter of 0.4–1.5 cm] and 35 benign nodules (maximum diameter 0.6–2.8 cm); 27 were nodular goiters, 4 were thyroid adenomas, and 4 were Hashimoto's thyroiditis.

SMI and CDFI results

There were significant differences observed between SMI and CDFI outcomes in the inspection of blood flow in benign and malignant nodules (*Table 1*). SMI was more sensitive in detecting low-velocity flow compared to CDFI (*Tables 1-3*). Type II and IV flow could be easily seen with SMI in benign nodules compared to CDFI, but the differences were statistically significant only for type II (*Table 2* and *Figure 1*). Meanwhile, SMI could detect type III flow in malignant nodules (*Table 3* and *Figure 2*).

CEUS results

Malignant nodules showed low enhancement by CEUS, whereas benign nodules showed equal or high enhancement. There was a significant difference in perfusion inconsistency between benign and malignant

Table 3 Assessment of the abundance of malignant nodules classified according to Kim *et al.*

Group	TI-RADS classification				χ^2	P
	I	II	III	IV		
CDFI	27	4	7	2	24.085	0.000
SMI	5	5	26	4		
χ^2	25.208	0.125	18.620	0.180		
P	0.000	0.723	0.000	0.671		

TI-RADS, Thyroid Imaging Reporting and Data System; CDFI, color Doppler imaging; SMI, superb micro-vascular imaging.

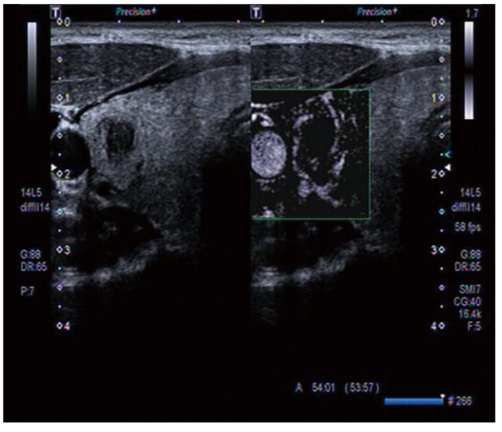

Figure 1 Nodular goiter, peripheral rim type blood flow shown by SMI with Kim Type II flow. SMI, superb micro-vascular imaging.

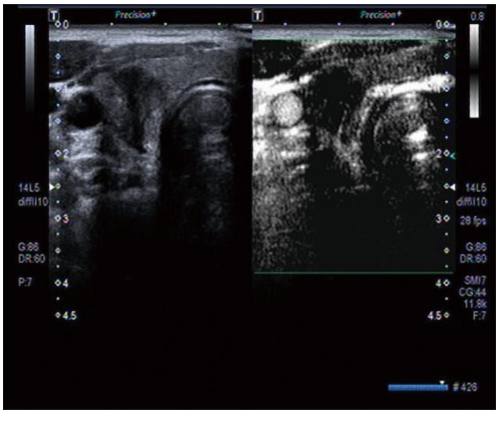

Figure 2 Papillary thyroid carcinoma, perforated branch flow shown by SMI with Kim Type III flow. SMI, superb micro-vascular imaging.

thyroid nodules, and no nodule showed a lack of enhancement (*Table 4*). Rim type enhancement was included in iso-enhancement and hyper-enhancement. Among the 35 benign nodules, three exhibited rim enhancement, whereas the 40 malignant nodules showed no rim enhancement. The rim enhancement ratio between the two groups showed no significant difference (χ^2=1.688, P=0.194).

New and old TI-RADS classification

After using CDFI, SMI, CEUS, and CEUS+SMI for the new TI-RADS classification, the subclass ratios of downgraded benign nodules were about 1/3, 2/3, 4/5, and 3/5, while the subclass with upgraded ratios of malignant nodules had ratios of approximately 1/4, 1/2, 3/5, and 1/2, respectively (*Table 5*). Few malignant nodules were present in the downgraded subclass, whereas few benign nodules were present in the upgraded subclass.

New and old TI-RADS classification AUC and results of diagnostic efficiency

Risk-scoring models were built, and the results of their diagnostic efficacy are summarized in *Table 6*. The AUC values for the new TI-RADS were 0.690 for CDFI, 0.840 for SMI, 0.910 for CEUS, and 0.903 for SMI + CEUS. CEUS had the highest diagnostic value among the three techniques. Joint inspection using SMI and CEUS provided a certain advantage in terms of sensitivity, yet the overall accuracy was equal to that of CEUS alone. Except for CDFI, the AUCs of the new TI-RADS were significantly higher than those of the old TI-RADS (*Table* 7 and *Figure 3*). Among all AUCs for the new TI-RADS, the AUC of CDFI was the lowest. The AUC of CEUS + SMI was higher than that of SMI alone, and was essentially equivalent to CEUS alone. Furthermore, the difference between the AUC for CEUS and SMI was significant.

Risk-scoring model

Univariate analysis showed that blur border/spicular/irregular shape, microcalcifications, central blood flow, and perforating vessels detected by SMI, along with nodule hypo-enhancement were related to thyroid cancer (*Table 8*). Multivariate analysis revealed that perforating vessels and

Table 4 CEUS manifestations compared with pathological results (cases)

Group	CEUS manifestations			Z	P
	Hypoperfusion	Isoperfusion	Hyperperfusion		
Benign nodules	3	14	18	6.302	0.000
Malignant nodules	33	5	2		
χ^2	40.874	7.463	20.576		
P	0.000	0.006	0.000		

CEUS, contrast-enhanced ultrasound.

Table 5 New and old TI-RADS classifications compared with pathological results

Pathological results	Old TI-RADS 4a4b4c	New TI-RADS by CDFI 34a4b4c5	New TI-RADS by SMI 34a4b4c5	New TI-RADS by CEUS 34a4b4c5	New TI-RADS by CEUS + SMI 34a4b4c5
Benign nodules	3,140	1,021,400	237,500	293,210	217,610
Malignant nodules	24,142	421,591	5,912,122	3,421,102	1,221,142

TI-RADS, Thyroid Imaging Reporting and Data System; CDFI, color Doppler imaging; SMI, superb micro-vascular imaging; CEUS, contrast-enhanced ultrasound.

Table 6 Diagnostic efficacy results

Classification standard	AUC	P	Sensitivity	Specificity	PPV	NPV	Accuracy
Old TI-RADS	0.646	0.030	40.00	88.57	80.00	56.36	62.67
New TI-RADS by CDFI	0.690	0.005	37.50	88.57	78.95	55.36	61.33
New TI-RADS by SMI	0.840	0.000	65.00	85.71	83.87	85.71	74.67
New TI-RADS by CEUS	0.910	0.000	82.50	91.43	91.67	82.05	86.67
New TI-RADS by CEUS+SMI	0.903	0.000	92.5	80.00	84.09	90.32	86.67

AUC, area under the curve; TI-RADS, Thyroid Imaging Reporting and Data System; CDFI, color Doppler imaging; SMI, superb micro-vascular imaging; CEUS, contrast-enhanced ultrasound.

hypo-enhancement were independent risk factors (*Table 9*).

Discussion

Numerous studies have confirmed that vascular imaging in the prediction of benign and malignant thyroid nodules is crucial. In this study, we used the three vascular imaging techniques of CDFI, CEUS, and SMI for the first time to reclassify and correct the subclass of TI-RADS 4 nodules that were included in the study. A risk score model was established to consider the value of flow characteristics in diagnosing thyroid nodules. A comparative study between old and new TI-RADS classifications showed significant differences between these two approaches.

CEUS could reveal blood perfusion in the tissue in real time. In CEUS analysis, high perfusion indicates that a tumor has an extensive microvasculature, whereas a low perfusion suggests a lower degree of microvasculature. Consistent with previous reports, here we showed that malignant nodules mainly displayed hypo-enhancement (13-15), which can be linked to compact fibrosis, functional inefficiency of new vessels, growth heterogeneity, and neovascular damage by tumor cells. Benign nodules typically manifested with hyper-enhancement or iso-enhancement, and the blood supply to these nodules was similar to that in peripheral normal tissue due to the dominance of follicular structures within the benign nodules. The diagnostic accuracy of the new TI-RADS obtained by

Table 7 Pairwise comparison of AUC

Comparison between classification standard	Z	P
Old TI-RADS and new TI-RADS by CDFI	1.322	0.1862
Old TI-RADS and new TI-RADS by SMI	5.063	0.000
Old TI-RADS and new TI-RADS by CEUS	6.491	0.000
Old TI-RADS and new TI-RADS by CEUS+SMI	6.775	0.000
New TI-RADS by CDFI and SMI	4.526	0.000
New TI-RADS by CDFI and CEUS	5.468	0.000
New TI-RADS by CDFI and CEUS+SMI	5.369	0.000
New TI-RADS by SMI and CEUS	2.375	0.0175
New TI-RADS by SMI and CEUS+SMI	2.164	0.0365
New TI-RADS by CEUS and CEUS+SMI	0.371	0.7109

AUC, area under the curve; TI-RADS, Thyroid Imaging Reporting and Data System; CDFI, color Doppler imaging; SMI, superb micro-vascular imaging; CEUS, contrast-enhanced ultrasound.

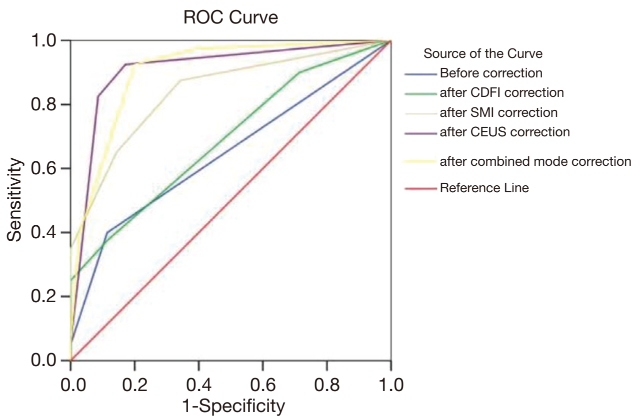

Figure 3 AUC of new and old TI-RADS classifications. AUC, area under the curve; TI-RADS, Thyroid Imaging Reporting and Data System.

CEUS correction was improved, particularly with respect to enhanced sensitivity, which was largely consistent with a study by Zhang *et al.* (16) showing that the malignant rate of nodules below the 4a subclass was decreased, whereas the malignant rate of nodules in subclass 4b and higher was increased compared to the earlier TI-RADS. Although CEUS was associated with high diagnostic accuracy, overlapping enhancement patterns existed between benign and malignant nodules. In the present study, two cases with Hashimoto's thyroiditis and one with nodular goiter exhibited heterogeneity and hypoenhancement that resulted in the absence of contrast agent in the lesion centers that had large areas of scarring. Meanwhile, seven papillary thyroid cancers (PTC) manifested with hyper-enhancement or iso-enhancement, which could have been due to the following: (I) an abundant blood supply that was available in the tumor itself; and/or (II) high expression levels of proangiogenic factors that could promote angiogenesis and tumor tissue differentiation, resulting in perfusion that is similar to or increased relative to normal thyroid tissue. Such nodules are generally suggestive of an abundance of nourishing vessels, and they tend to grow vigorously with strong invasion. Indeed, Hong *et al.* (17) reported an increased incidence of capsular invasion or extra-capsular fibrous and adipose tissue invasion, as well as lymph node metastasis in the central cervical region that was associated with hyper-enhancement and iso-enhancement PTC relative to PTC with hypo-enhancement. Although the significance of rim enhancement for benign nodules is unclear, fewer nodules in this study displayed rim enhancement, which could reflect the selective deviation for all nodules in the group that were classified as TI-RADS 4.

SMI could clearly and conveniently display low-velocity blood that CDFI could not, which could be a better depiction of true tumor blood flow and is consistent with findings in a study by Forsberg *et al.* (18). Our comparison of SMI, CDFI, and CEUS indicated the following: (I) our findings were consistent with results of Phuttharak *et al.* (19,20) showing different types of vascular distributions in benign and malignant nodules inspected by SMI, wherein peripheral flow and mixed flow were often discovered

Table 8 Results of univariate regression analysis

Variables	Benign nodules	Malignant nodules	χ^2	P
Blurred edge/micro-leaflet/irregular morphology (yes/no)	26/9	20/20	4.642	0.031
Aspect ratio >1 (yes/no)	6/29	14/26	3.044	0.081
Microcalcification (yes/no)	7/28	24/16	12.317	0.000
Central blood flow (yes/no)	5/30	26/14	19.799	0.000
Perforating vessels (yes/no)	1/34	18/22	17.527	0.000
Hypo-enhancement (yes/no)	3/32	33/7	40.874	0.000

Table 9 Results of multivariate regression analysis

Variables	B	Wald	P	OR	95% CI for OR	
					Lower	Upper
Blurred edge/irregular shape	–0.327	0.114	0.736	0.721	0.108	4.819
Microcalcification	1.084	1.372	0.241	2.958	0.482	18.151
Central blood flow	0.231	0.040	0.841	1.260	0.131	12.100
Perforating vessels	3.477	4.445	0.035	32.374	1.277	820.498
Hypo-enhancement	3.936	16.847	0.000	51.213	7.819	335.456
Constant	–2.493	6.344	0.012	0.083		

in benign nodules and central flow was mainly found in malignant nodules; (II) the diagnostic accuracy could be markedly improved by applying SMI compared with the original TI-RADS and in the new TI-RADS using CDFI, although CEUS yielded better results than SMI. This finding demonstrated the value of SMI for diagnosing nodules, even though this approach was not as good as CEUS, which is consistent with conclusions of Lu *et al.* (21); (III) the accuracy of SMI in diagnosing PTC through identification of perforating vessels was similar to that of CEUS. After assessment of risk factors, perforating vessels and hypo-enhancement were confirmed to be independent risk factors for PTC. Thus, although SMI was inferior to CEUS for the inspection of nodules, SMI nonetheless had advantages for detecting the presence of perforating vessels within the nodules. This finding is in agreement with that by Wu *et al.* (9), who concluded that SMI better displayed integral vascular networks and was of great value in predicting the nature of such networks. In contrast, CEUS could not detect true perforating vessels, which could be attributed to its high sensitivity to blood flow.

Our results are partly in line with those of Gabriel *et al.* (22), who pointed out that additional information could be acquired by combining CEUS and SMI. The SMI gray-scale pattern highlights the flow signal by suppressing 2-D tissue information, in turn clarifying the flow branch and direction within the tumor. In comparison, CEUS was superior in reflecting tumor perfusion characteristics through the use contrast agents having distinct flow characteristics that can provide diagnostic benefits. As we indicated in this study, CEUS + SMI had higher sensitivity and lower specificity compared with CEUS or SMI alone, suggesting that the joint model could have a certain rate of misdiagnosis that might be related to an incorrect setting of the joint diagnostic criteria. If the subclasses of the new TI-RADS obtained using CEUS and SMI jointly are not consistent, the diagnostic outcomes may be debated, although when a nodule subclass is downgraded by CEUS alone and upgraded by joint analysis, the nodular diagnosis assigned by CEUS results should be given preference. Conversely, if the subclass is downgraded by SMI and upgraded after joint analysis, we recommend that the joint outcomes be preferred.

Our study has several potential limitations. First, fewer pathological types were explored and the sample size was small, such that some degree of selection bias was unavoidable. This requires more communication and coordination between us and the clinic, and more biopsy before surgery. So that we can collect more cases for research. The size of the selected benign and malignant nodules differed in that the benign nodules were larger, which could have affected the diagnostic efficiency. Meanwhile, the SMI approach only assessed the flow distribution, and this technology is less well-characterized. Furthermore, CEUS only considered the enhancement intensity, and other parameters, such as entry time and extinction time, require additional analysis. Operators must carefully examine the 2-D images to determine whether microcalcification is present to avoid mistaking microcalcification for a flow signal.

Conclusions

In summary, in a comparison of the three ultrasonic flow imaging technologies, CEUS had the highest sensitivity and accuracy for distinguishing benign from malignant thyroid nodules. Although the diagnostic performance of SMI was limited, its sensitivity increased when combined CEUS, indicating that SMI could be a promising tool for diagnosis of thyroid nodule malignancies.

Acknowledgments

Funding: None.

Footnote

Reporting Checklist: The authors have completed the STARD reporting checklist. Available at http://dx.doi.org/10.21037/gs-20-641

Data Sharing Statement: Available at http://dx.doi.org/10.21037/gs-20-641

Conflicts of Interest: The authors have completed the ICMJE uniform disclosure forms (available at http://dx.doi.org/10.21037/gs-20-6410. The authors have no conflicts of interest to declare.

Ethical Statement: The authors are accountable for all aspects of the work in ensuring that questions related to the accuracy or integrity of any part of the work are appropriately investigated and resolved. Written informed consent was obtained from all study subjects. The study was conducted in accordance with the Declaration of Helsinki (as revised in 2013), and was approved by Shanghai East Hospital, Tongji University School of Medicine (No. 102).

References

1. Horvath E, Majlis S, Rossi R, et al. An ultrasonogram reporting system for thyroid nodules stratifying cancer risk. J Clin Endocrinol Metab 2009;94:1748-51.
2. American College of Radiology. Breast imaging reporting and data system, breast imaging atlas. 4th ed. Reston, Va: American College of Radiology, 2003.
3. Spira D, Neumeister H, Spira SM, et al. Assessment of tumor vascularity in lung cancer using volume perfusion CT (VPCT) with histopathologic comparison: a further step toward an individualized tumor characterization. J Comput Assist Tomogr 2013;37:15-21.
4. Zhan J, Diao XH, Jin JM, et al. Superb Microvascular Imaging—A new vascular detecting ultrasonographic technique for avascular breast masses: Apreliminary study. Eur J Radiol 2016;85:915-21.
5. Swinburne NC, Schefflein J, Sakai Y, et al. Machine learning for semi-automated classification of glioblastoma, brain metastasis and central nervous system lymphoma using magnetic resonance advanced imaging. Ann Transl Med 2019;7:232.
6. Machado P, Segal S, Lyshchik A, et al. A novel microvascular flow technique: initial results in thyroids. Ultrasound Q 2016;32:67-74.
7. Park JY, Lee HJ, Jang HW, et al. A proposal for a thyroid imaging reporting and data system for ultrasound features of thyroid carcinoma. Thyroid 2009;19:1257-64.
8. Kwak JY, Han KH, Yoon JH, et al. Thyroid imaging reporting and data system for US features of nodules: a step in establishing better stratification of cancer risk. Radiology 2011;260:892-9.

9. Wu C, Zhu L, Chen W, et al. Study on the hemodynamic changes in solid thyroid nodules by ultrasound contrast quantitative analysis. Zhonghua Yi Xue Za Zhi 2015;95:3519-22.
10. Zhou Q, Jiang J, Shang X, et al. Correlation of contrast-enhanced ultrasonographic features with microvessel density in papillary thyroid carcinomas. Asian Pac J Cancer Prev 2014;15:7449-52.
11. Wendl CM, Janke M, Jung W, et al. Contrast-enhanced ultrasound with perfusion analysis for the identification of malignant and benign tumours of the thyroid gland. Clin Hemorheol Microcirc 2015;63:113-21.
12. De Nicola H, Szejnfeld J, Logullo AF, et al. Flow pattern and vascular resistive index as predictors of malignancy risk in thyroid follicular neoplasms. J Ultrasound Med 2005;24:897-904.
13. Bartolotta TV, Midiri M, Galia M, et al. Qualitative and quantitative evaluation of solitary thyroid nodules with contrast enhanced ultrasound: initial results. Eur Radiol 2006;16:2234-41.
14. Cantisani V, Consorti F, Guerrisi A, et al. Prospective comparative evaluation of quantitative-elastosonography (Q-elastography) and contrast-enhanced ultrasound for the evaluation of thyroid nodules: preliminary experience. Eur J Radiol 2013;82:1892-8.
15. Debnam JM, Vu T, Sun J, et al. Vascular flow on doppler sonography may not be a valid characteristic to distinguish colloid nodules from papillary thyroid carcinoma even when accounting for nodular size. Gland Surg 2019;8:461-8.
16. Zhang Y, Zhou P, Tian SM, et al. Usefulness of combined use of contrast-enhanced ultrasound and TI-RADS classification for the differentiation of benign from malignant lesions of thyroid nodules. Eur Radiol 2017;27:1527-36.
17. Hong YR, Yan CX, Mo GQ, et al. Conventional US, elastography, and contrast enhanced US features of papillary thyroid microcarcinoma predict central compartment lymph node metastases. Sci Rep 2015;5:7748.
18. Forsberg F, Machado P, Segal S, et al. Microvascular Blood Flow in the Thyroid:Preliminary Results with a Novel Imaging Technique. Ultrasonics Symposium IEEE 2014;10:2237-40.
19. Phuttharak W, Somboonporn C, Hongdomnern G. Diagnostic performance of gray-scale versus combined gray-scale with colour doppler ultrasonography in the diagnosis of malignancy in thyroid nodules. Asian Pac J Cancer Prev 2009;10:759-64.
20. Hornung M, Jung EM, Georgieva M, et al. Detection of microvascularization of thyroid carcinomas using linear high resolution contrast-enhanced ultrasonography (CEUS). Clin Hemorheol Microcirc 2012;52:197-203.
21. Lu R, Meng Y, Zhang Y, et al. Superb microvascular imaging (SMI) compared with conventional ultrasound for evaluating thyroid nodules. BMC Med Imaging 2017;17:65.
22. Gabriel M, Tomczak J, Snoch-Ziółkiewicz M, et al. Comparison of Superb Micro-Vascular Ultrasound Imaging (SMI) and Contrast-Enhanced Ultrasound (CEUS) for Detection of Endoleaks After Endovascular Aneurysm Repair (EVAR). Am J Case Rep 2016;17:43-6.

(English Language Editor: J. Gray)

Cite this article as: Zhang L, Gu J, Zhao Y, Zhu M, Wei J, Zhang B. The role of multimodal ultrasonic flow imaging in Thyroid Imaging Reporting and Data System (TI-RADS) 4 nodules. Gland Surg 2020;9(5):1469-1477. doi: 10.21037/gs-20-641

